SLAC-PUB-16108

Understanding the charmed states recently observed by the LHCb and BaBar Collaborations in the quark model

Qi-Fang Lü and De-Min Li*

Department of Physics, Zhengzhou University, Zhengzhou, Henan 450001, China

Comparing the expected spectroscopy in the relativistic quark model and the predicted strong decays in the $^3P_0$ model employing the realistic wave functions from the relativistic quark model with the measured properties of the LHCb and BaBar charmed states, we find that the masses and strong decays of these charmed states can be reasonably explained in the conventional $q\bar{q}$ picture, and therefore suggest that the $D(2550)/D_J(2580)$, $D^*(2600)/D_J^*(2650)$, $D(2750)/D_J(2740)$, $D^*(2760)/D_J^*(2760)$, $D_J(3000)$, and $D_J^*(3000)$ can be identified as the $D(2^1S_0)$, $D(2^3S_1)$, $D_2'(1D)$, $D(1^3D_3)$, $D(3^1S_0)$, and $D(1^3F_4)$, respectively.

PACS numbers: 12.39.Ki, 14.40.Lb, 12.38.Lg, 13.25.Ft

I. INTRODUCTION

In 2013, the LHCb Collaboration reported several D_J resonances by studying the $D\pi$ and $D^*\pi$ final states in pp collisions[1]. The $D_J(2580)$, $D_J^*(2650)$, $D_J(2740)$, and $D_J(3000)$ were observed in the $D^{*+}\pi^-$ channel, the $D_J^*(3000)$ was observed in the $D^+\pi^-$ channel, and the $D^*(2760)$ was observed in both the $D^{*+}\pi^-$ and $D^+\pi^-$ channels. The helicity-angle distributions indicate that the $D_J(2580)$, $D_J(2740)$, and $D_J(3000)$ are the unnatural parity resonances [$P = (-1)^{(J+1)}$], while the $D_J^*(2650)$ and $D_J^*(2760)$ are the natural parity resonances [$P = (-1)^J$]. The observation of the $D_J^*(3000)$ in the $D^+\pi^-$ channel makes this state should be a natural parity resonance.

In 2010, the BaBar Collaboration also reported several charmed states by analyzing the $D\pi$ and $D^*\pi$ systems in inclusive $e^+e^- \to c\bar{c}$ interactions[2]. The $D(2550)$ and $D(2750)$ were observed in the $D^{*+}\pi^-$ channel, the $D^*(2760)$ was observed in the $D^+\pi^-$ channel, and the

*Electronic address: lidm@zzu.edu.cn

SLAC National Accelerator Laboratory, 2575 Sand Hill Road, Menlo Park, CA 94025

This work was supported at SLAC by the US Department of Energy under contract DE-AC02-76SF00515 and HEP.

$D^*(2600)$ was observed in both the $D^{*+}\pi^-$ and $D^+\pi^-$ channels. The helicity-angle distributions indicate that the $D(2550)$ and $D(2750)$ are the unnatural parity resonances, while the $D^*(2600)$ is the natural parity resonance. The observation of the $D^*(2760)$ in the $D^+\pi^-$ channel shows that it should be a natural parity resonance. The measured masses and widths of these LHCb and BaBar charmed states mentioned above are listed in Table I. Based on the masses, decay modes, and helicity-angle distributions, we regard that the BaBar charmed states $D(2550)$, $D^*(2600)$, $D(2750)$, and $D^*(2760)$ are in fact compatible with the LHCb states $D_J(2580)$, $D_J^*(2650)$, $D_J(2740)$, and $D_J^*(2760)$, respectively. The average values of the LHCb and BaBar measurements are also shown in Table I.

Apart from the ordinary $q\bar{q}$ states, other exotic states such as glueballs, hybrids, and multiquark systems are expected to exist in the framework of Quantum Chromodynamics (QCD). The identification of these exotic states requires to understand well the conventional $q\bar{q}$ meson spectroscopy both theoretically and experimentally. To a large extent, our knowledge of meson spectroscopy is based on some phenomenological QCD motivated models such as quark models which are widely accepted to offer the most complete description of meson properties and are probably the most successful phenomenological models of hadron structures[3].

According to the PDG[4], the low-mass charmed mesons $D(1^1S_0)$, $D(1^3S_1)$, $D(1^3P_1)$, $D(1^1P_1)$, $D(1^3P_0)$, and $D(1^3P_2)$ predicted by quark models are well established experimentally, however, many other higher radial and orbital excitations of D mesons predicted by quark models have not yet been established. These charmed states recently reported by the LHCb Collaboration and the BaBar Collaboration are clearly of importance to improve our understanding of the charmed meson spectroscopy. The possible $q\bar{q}$ quark-model assignments for these observed charmed states have been studied in the context of various models such as the chiral quark model[5–7], the heavy meson effective theory[8–10], and the $^3P_0$ model with the simple harmonic oscillator wave functions[11–15] or the nonrelativistic quark model wave functions[16], and other approaches[17–19]. It is also natural and necessary to exhaust the possible $q\bar{q}$ descriptions before restoring to more exotic assignments. The theoretical predictions for these states are not completely consistent with the measured properties and there is not yet a consensus on the assignments of these states. Therefore, in order to deeply understand these newly reported charmed states, further test calculations against the experimental measurements are still required.

In this work, we shall compare the observed properties of the LHCb and BaBar charmed

TABLE I: The neutral charge resonances observed by the LHCb Collaboration[1] and the BaBar Collaboration[2]. The N and UN stand for the natural parity and unnatural parity, respectively.

State	Channel	Parity	Property (MeV)	Average (MeV)
$D_J(2580)^0$[1]	$D^{*+}\pi^-$	UN	Mass: $2579.5 \pm 3.4 \pm 5.5$	Mass: $2559.5 \pm 2.8 \pm 4.4$
			Width: $177.5 \pm 17.8 \pm 46.0$	
$D(2550)^0$[2]	$D^{*+}\pi^-$	UN	Mass: $2539.4 \pm 4.5 \pm 6.8$	Width: $153.8 \pm 10.7 \pm 23.9$
			Width: $130 \pm 12 \pm 13$	
$D_J^*(2650)^0$[1]	$D^{*+}\pi^-$	N	Mass: $2649.2 \pm 3.5 \pm 3.5$	Mass: $2628.9 \pm 2.1 \pm 2.1$
			Width: $140.2 \pm 17.1 \pm 18.6$	
$D^*(2600)^0$[2]	$D^{*+}\pi^-$, $D^+\pi^-$	N	Mass: $2608.7 \pm 2.4 \pm 2.5$	Width: $116.6 \pm 9.1 \pm 11.3$
			Width: $93 \pm 6 \pm 13$	
$D_J(2740)^0$[1]	$D^{*+}\pi^-$	UN	Mass: $2737.0 \pm 3.5 \pm 11.2$	Mass: $2744.7 \pm 1.9 \pm 5.8$
			Width: $73.2 \pm 13.4 \pm 25.0$	
$D(2750)^0$[2]	$D^{*+}\pi^-$	UN	Mass: $2752.4 \pm 1.7 \pm 2.7$	Width: $72.1 \pm 7.4 \pm 13.7$
			Width: $71 \pm 6 \pm 11$	
$D_J^*(2760)^0$[1]	$D^{*+}\pi^-$, $D^+\pi^-$	N	Mass: $2761.1 \pm 5.1 \pm 6.5$	Mass: $2762.2 \pm 2.8 \pm 3.5$
			Width: $74.4 \pm 3.4 \pm 37.0$	
$D^*(2760)^0$[2]	$D^+\pi^-$	N	Mass: $2763.3 \pm 2.3 \pm 2.3$	Width: $67.6 \pm 3.1 \pm 18.6$
			Width: $60.9 \pm 5.1 \pm 3.6$	
$D_J(3000)^0$[1]	$D^{*+}\pi^-$	UN	Mass: 2971.8 ± 8.7	Mass: 2971.8 ± 8.7
			Width: 188.1 ± 44.8	Width: 188.1 ± 44.8
$D_J^*(3000)^0$[1]	$D^+\pi^-$	N	Mass: 3008.1 ± 4.0	Mass: 3008.1 ± 4.0
			Width: 110.5 ± 11.5	Width: 110.5 ± 11.5

states with the mass predictions of the relativistic quark model and strong decay predictions of the $^3P_0$ model employing the relativistic quark model wave functions to determine their spectroscopic assignments.

This work is organized as follows. In Sec. II, we calculate the charmed meson masses in the Godfrey and Isgur (GI) relativized quark model and give the possible assignments for these charmed states based on their observed masses and decay modes. In Sec. III, we investigate

the strong decays of these states for different possible assignments in the $^3P_0$ model using the realistic wave functions from the GI quark model. The summary is given in the last section.

II. MASSES

To understand the properties of the charmed mesons, we shall discuss their masses in a relativistic quark model proposed by Godfrey and Isgur[20]. In this model, the total Hamiltonian is

$$\tilde{H} = H_0 + \tilde{V}(\boldsymbol{p}, \boldsymbol{r}), \tag{1}$$

$$H_0 = (\boldsymbol{p}^2 + m_1^2)^{1/2} + (\boldsymbol{p}^2 + m_2^2)^{1/2}, \tag{2}$$

$$\tilde{V}(\boldsymbol{p}, \boldsymbol{r}) = \tilde{H}_{12}^{\rm conf} + \tilde{H}_{12}^{\rm cont} + \tilde{H}_{12}^{\rm ten} + \tilde{H}_{12}^{\rm so}, \tag{3}$$

where $\tilde{H}_{12}^{\rm conf}$ includes the spin-independent linear confinement and Coulomb-type interactions; $\tilde{H}_{12}^{\rm cont}$, $\tilde{H}_{12}^{\rm ten}$, and $\tilde{H}_{12}^{\rm so}$ are the color contact term, color tensor interaction, and spin-orbit interaction, respectively. The details of this model and the explicit form of these interactions can be found in Appendix A of Ref.[20].

The spin-orbit interaction term $\tilde{H}_{12}^{\rm so}$ can decompose into symmetric $\tilde{H}_{(12)}^{\rm so}$ and antisymmetric $\tilde{H}_{[12]}^{\rm so}$. The antisymmetric $\tilde{H}_{[12]}^{\rm so}$ can cause the the mixing of the charmed mesons with different total spins but with the same total angular momentum such as $D(n^3L_L)$ and $D(n^1L_L)$. Consequently, the two physical states $D_L(nL)$ and $D'_L(nL)$ can be described by[20, 21]

$$\begin{pmatrix} D_L(nL) \\ D'_L(nL) \end{pmatrix} = \begin{pmatrix} \cos\theta_{nL} & \sin\theta_{nL} \\ -\sin\theta_{nL} & \cos\theta_{nL} \end{pmatrix} \begin{pmatrix} D(n^1L_L) \\ D(n^3L_L) \end{pmatrix}, \tag{4}$$

where the θ_{nL} is the mixing angle.

The total Hamiltonian $\tilde{H}$ can be divided into the diagonal part $\tilde{H}_{\rm diag} = H_0 + \tilde{H}_{12}^{\rm conf} + \tilde{H}_{12}^{\rm cont} + (\tilde{H}_{12}^{\rm ten})_{\rm diag} + \tilde{H}_{(12)}^{\rm so}$ and the off-diagonal part $\tilde{H}_{\rm off} = \tilde{H}_{[12]}^{\rm so} + (\tilde{H}_{12}^{\rm ten})_{\rm off}$, where $(\tilde{H}_{12}^{\rm ten})_{\rm off}$ can cause $^3L_J \leftrightarrow {}^3L'_J$ mixing and is neglected in the present work. We use the Gaussian expansion method [22] to solve the Hamiltonian (1). To actually perform the calculations, we first diagonalize $\tilde{H}_{\rm diag}$ in the Gaussian function basis to obtain the masses and wave functions for the unmixed D mesons, then in the basis $|n^{2S+1}L_J\rangle$, we diagonalize the off-diagonal part $\tilde{H}_{[12]}^{\rm so}$, which is treated as the perturbative term, to obtain the masses of the mixed D_L and D'_L mesons. In this procedure, the mixing angle θ_{nL} can be obtained. The values of the model parameters used in our calculations are taken from Ref.[20].

We apply the GI quark model to calculate the mass spectra of the $1S$, $2S$, $3S$, $1P$, $2P$, $3P$, $1D$, $2D$, $3D$, $1F$, $2F$, $3F$, $1G$, and $2G$ states. The masses of the $1S$, $2S$, $1P$, $1D$, and $1F$ states in the origin paper of Godfrey and Isgur[20] are well reproduced. Our calculated D meson masses are listed in Table II. The predictions of some other relativistic quark models[23–25] are also listed. We do not list the mass predictions of Ref.[13], where the masses of the $D_L(nL)$ and $D'_L(nL)$ are not calculated due to the $\tilde{H}^{\rm so}_{[12]}$ term being neglected and the unmixed D meson spectra are almost the same as our present calculations. These predictions from different relativistic quark models give us a mass range for the corresponding D meson, which can restrict the possible assignments for the reported charmed states.

The predicted mass ranges from different relativistic quark models and information of the observed charmed states are depicted in Fig. 1. Clearly, the masses of the D, $D^*(2007)$, $D_0^*(2400)$, $D_1(2420)$, $D_1(2430)$, and $D_2^*(2460)$ as the well-established ground charmed mesons are well reproduced. The $D(2550)/D_J(2580)$ and $D^*(2600)/D_J^*(2650)$ lie within the $D(2^1S_0)$ and $D(2^3S_1)$ mass ranges, respectively. The $D(2750)/D_J(2740)$ and $D^*(2760)/D_J^*(2760)$ lie within the $1D$ states mass ranges. The $D_J(3000)$ and $D_J^*(3000)$ lie close to the mass ranges of the $3S$, $2P$, and $1F$ states. We regard the BaBar state $D^*(2760)$ and the LHCb state $D_J^*(2760)$ as the same state, so the observation of the $D_J^*(2760)$ in the $D^{*+}\pi$ channel excludes the $D(2^3P_0)$ assignment, although the expected $D(2^3P_0)$ mass range is very close to the $D^*(2760)/D_J^*(2760)$ mass. We don't consider the possibility of the $D_J^*(3000)$ and $D_J(3000)$ being the the $2D$ states, since the predicted $2D$ mass ranges are at least 130 MeV higher than the $D_J^*(3000)$ and $D_J(3000)$ masses. Based on the mass and the parity, our tentative assignments for these newly reported charmed states are listed in Table III. Below, we shall focus on these possible assignments. It should be noted that the mass information alone is insufficient to classify these charmed states, so their decay behaviors also need to be compared with model expectations. In the next section, we shall discuss the strong decays in the $^3P_0$ model employing the wave functions from the GI quark model.

TABLE II: The D meson masses in MeV from different relativistic quark models. The mixing angles of $D_L - D'_L$ obtained in this work are $\theta_{1P} = -25.5°$, $\theta_{2P} = -29.4°$, $\theta_{3P} = -27.7°$, $\theta_{1D} = -38.2°$, $\theta_{2D} = -37.5°$, $\theta_{3D} = -36.8°$, $\theta_{1F} = -39.5°$, $\theta_{2F} = -39.4°$, $\theta_{3F} = -39.4°$, $\theta_{1G} = -40.2°$, and $\theta_{2G} = -40.3°$. A dash denotes that the corresponding mass was not calculated in the corresponding reference.

State	This work	ZVR[23]	DE[24]	EFG[25]	State	This work	ZVR[23]	DE[24]	EFG[25]
$D(1^1S_0)$	1874	1850	1868	1871	$D(2^3D_3)$	3227	3190	–	3335
$D(1^3S_1)$	2038	2020	2005	2010	$D(3^3D_1)$	3595	–	–	–
$D(2^1S_0)$	2583	2500	2589	2581	$D_2(3D)$	3576	–	–	–
$D(2^3S_1)$	2645	2620	2692	2632	$D'_2(3D)$	3610	–	–	–
$D(3^1S_0)$	3068	2980	3141	3062	$D(3^3D_3)$	3591	–	–	–
$D(3^3S_1)$	3111	3070	3226	3096	$D(1^3F_2)$	3132	3000	3101	3090
$D(1^3P_0)$	2398	2270	2377	2406	$D_3(1F)$	3109	3010	3074	3129
$D_1(1P)$	2455	2400	2417	2426	$D'_3(1F)$	3144	3030	3123	3145
$D'_1(1P)$	2467	2410	2490	2469	$D(1^3F_4)$	3113	3030	3091	3187
$D(1^3P_2)$	2501	2460	2460	2460	$D(2^3F_2)$	3491	3380	–	–
$D(2^3P_0)$	2932	2780	2949	2919	$D_3(2F)$	3462	3390	–	–
$D_1(2P)$	2925	2890	2995	2932	$D'_3(2F)$	3499	3410	–	–
$D'_1(2P)$	2961	2890	3045	3021	$D(2^3F_4)$	3466	3410	–	3610
$D(2^3P_2)$	2957	2940	3035	3012	$D(3^3F_2)$	3833	–	–	–
$D(3^3P_0)$	3344	3200	–	3346	$D_3(3F)$	3809	–	–	–
$D_1(3P)$	3329	3290	–	3365	$D'_3(3F)$	3843	–	–	–
$D'_1(3P)$	3362	3300	–	3461	$D(3^3F_4)$	3816	–	–	–
$D(3^3P_2)$	3356	3340	–	3407	$D(1^3G_3)$	3398	3240	–	3352
$D(1^3D_1)$	2816	2710	2795	2788	$D_4(1G)$	3365	3240	–	3403
$D_2(1D)$	2816	2740	2775	2806	$D'_4(1G)$	3400	3260	–	3415
$D'_2(1D)$	2845	2760	2833	2850	$D(1^3G_5)$	3362	–	–	3473
$D(1^3D_3)$	2833	2780	2799	2863	$D(2^3G_3)$	3722	–	–	–
$D(2^3D_1)$	3232	3130	–	3228	$D_4(2G)$	3687	–	–	–
$D_2(2D)$	3212	3160	–	3259	$D'_4(2G)$	3723	–	–	–
$D'_2(2D)$	3249	3170	–	3307	$D(2^3G_5)$	3685	–	–	3860

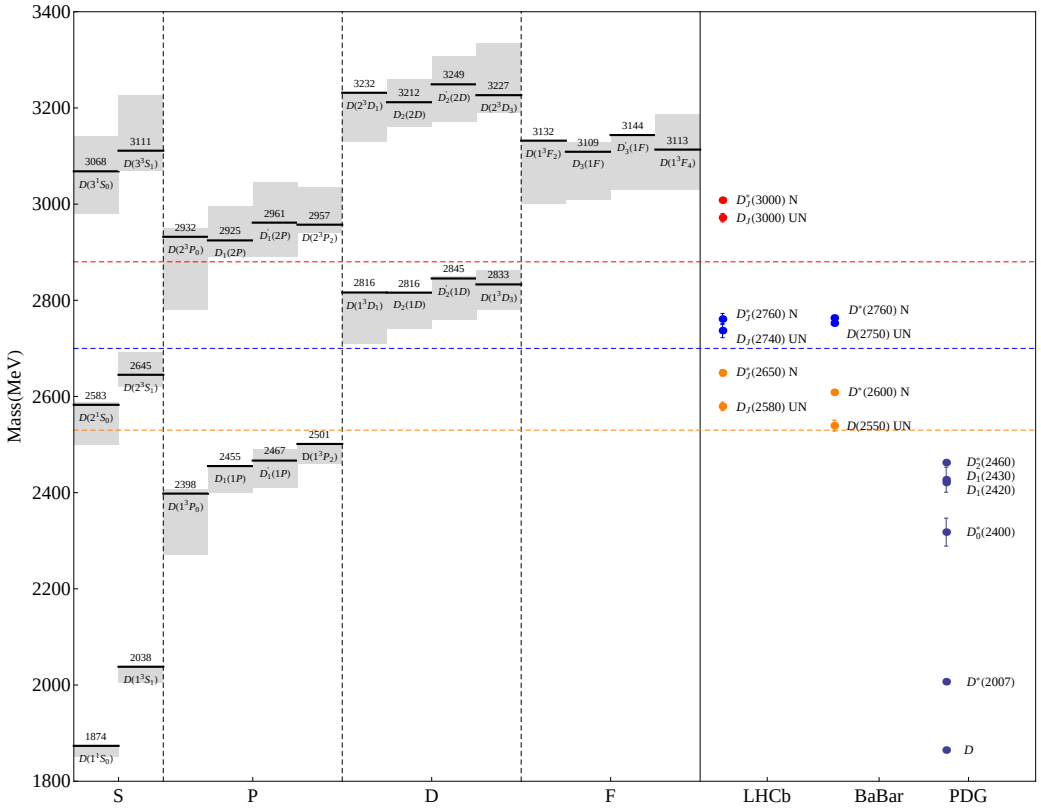

FIG. 1: The charmed meson spectrum. The solid lines are the GI quark model predictions and the shaded regions are the expected mass ranges from some other relativistic quark models[23–25]. The observed charmed states are also shown. The N and UN denote natural parity and unnatural parity, respectively.

TABLE III: Possible assignments for the LHCb and BaBar charmed states based on masses and decay modes

State	Possible assignments
$D(2550)/D_J(2580)$	$D(2^1S_0)$
$D^*(2600)/D_J^*(2650)$	$D(2^3S_1)$
$D(2750)/D_J(2740)$	$D_2(1D)$, $D_2'(1D)$
$D^*(2760)/D_J^*(2760)$	$D(1^3D_1)$, $D(1^3D_3)$
$D_J(3000)$	$D(3^1S_0)$, $D_1(2P)$, $D_1'(2P)$, $D_3(1F)$, $D_3'(1F)$
$D_J^*(3000)$	$D(3^3S_1)$, $D(2^3P_0)$, $D(2^3P_2)$, $D(1^3F_2)$, $D(1^3F_4)$

III. STRONG DECAYS

A. $^3P_0$ model

In this section, we employ the $^3P_0$ model to evaluate the Okubo-Zweig-Iizuka-allowed two-body strong decays of the initial state. The $^3P_0$ model, also known as the quark pair creation model, in which meson decay takes place through a quark-antiquark pair with the vacuum quantum number[26], has been extensively applied to study the strong decay of hadrons. There exists exhaustive literature on the $^3P_0$ model and some detailed reviews on the $^3P_0$ model can be found in Refs.[27–30]. Here we give the main ingredients of the $^3P_0$ model. Following the conventions in Ref.[31], the transition operator T of the decay $A \to BC$ in the $^3P_0$ model is given by

$$T = -3\gamma \sum_m \langle 1m1-m|00\rangle \int d^3\boldsymbol{p}_3 d^3\boldsymbol{p}_4 \delta^3(\boldsymbol{p}_3+\boldsymbol{p}_4)\mathcal{Y}_1^m\left(\frac{\boldsymbol{p}_3-\boldsymbol{p}_4}{2}\right)\chi^{34}_{1-m}\phi_0^{34}\omega_0^{34}b_3^\dagger(\boldsymbol{p}_3)d_4^\dagger(\boldsymbol{p}_4), \quad (5)$$

where γ is a dimensionless $q_3\bar{q}_4$ pair-production strength, and $\boldsymbol{p}_3$ and $\boldsymbol{p}_4$ are the momenta of the created quark q_3 and antiquark $\bar{q}_4$, respectively. ϕ_0^{34}, ω_0^{34}, and $\chi^{34}_{1,-m}$ are the flavor, color, and spin wave functions of the $q_3\bar{q}_4$, respectively. The solid harmonic polynomial $\mathcal{Y}_1^m(\boldsymbol{p}) \equiv |p|^1 Y_1^m(\theta_p,\phi_p)$ reflects the momentum-space distribution of the $q_3\bar{q}_4$.

The partial wave amplitude $\mathcal{M}^{LS}(\boldsymbol{P})$ for $A \to BC$ is expressed as

$$\begin{aligned}\mathcal{M}^{LS}(\boldsymbol{P}) \;=\; & \sum_{\substack{M_{J_B},M_{J_C},\\ M_S,M_L}} \langle LM_LSM_S|J_AM_{J_A}\rangle\langle J_BM_{J_B}J_CM_{J_C}|SM_S\rangle \\ & \times \int d\Omega\, Y^*_{LM_L}\mathcal{M}^{M_{J_A}M_{J_B}M_{J_C}}(\boldsymbol{P}), \end{aligned} \quad (6)$$

where $\mathcal{M}^{M_{J_A}M_{J_B}M_{J_C}}(\boldsymbol{P})$ is the helicity amplitude and defined by

$$\langle BC|T|A\rangle = \delta^3(\boldsymbol{P}_A-\boldsymbol{P}_B-\boldsymbol{P}_C)\mathcal{M}^{M_{J_A}M_{J_B}M_{J_C}}(\boldsymbol{P}). \quad (7)$$

The $|A\rangle$, $|B\rangle$, and $|C\rangle$ stand for the mock meson states. The mock meson $|A\rangle$ is defined by[32]

$$\begin{aligned}|A(n_A^{2S_A+1}L_{A\,J_AM_{J_A}})(\boldsymbol{P}_A)\rangle \;\equiv\; & \sqrt{2E_A}\sum_{M_{L_A},M_{S_A}} \langle L_AM_{L_A}S_AM_{S_A}|J_AM_{J_A}\rangle \\ & \times \int d^3\boldsymbol{p}_A \psi_{n_AL_AM_{L_A}}(\boldsymbol{p}_A)\chi^{12}_{S_AM_{S_A}}\phi_A^{12}\omega_A^{12} \\ & \times \left|q_1\left(\tfrac{m_1}{m_1+m_2}\boldsymbol{P}_A+\boldsymbol{p}_A\right)\bar{q}_2\left(\tfrac{m_2}{m_1+m_2}\boldsymbol{P}_A-\boldsymbol{p}_A\right)\right\rangle, \end{aligned} \quad (8)$$

where m_1 and m_2 ($\boldsymbol{p}_1$ and $\boldsymbol{p}_2$) are the masses (momenta) of the quark q_1 and the antiquark $\bar{q}_2$, respectively; $\boldsymbol{P}_A = \boldsymbol{p}_1 + \boldsymbol{p}_2$, $\boldsymbol{p}_A = \frac{m_2\boldsymbol{p}_1 - m_1\boldsymbol{p}_2}{m_1+m_2}$; $\chi^{12}_{S_A M_{S_A}}$, ϕ^{12}_A, ω^{12}_A, $\psi_{n_A L_A M_{L_A}}(\boldsymbol{p}_A)$ are the spin, flavor, color, and space wave functions of the meson A composed of $q_1\bar{q}_2$ with total energy E_A, respectively.

Various $^3P_0$ models exist in literature and typically differ in the choice of the pair-production vertex, the phase space conventions, and the meson wave functions employed. In this work, we restrict to the simplest vertex as introduced originally by Micu[26] which assumes a spatially constant pair-production strength γ, adopt the relativistic phase space as Ref.[31], and employ the realistic meson wave functions from the GI quark model. With the relativistic phase space, the decay width $\Gamma(A \to BC)$ in terms of the partial wave amplitude Eq. (6) is given by

$$\Gamma(A \to BC) = \frac{\pi P}{4M_A^2} \sum_{LS} |\mathcal{M}^{LS}(\boldsymbol{P})|^2, \tag{9}$$

where $P = |\boldsymbol{P}| = \sqrt{[M_A^2 - (M_B + M_C)^2][M_A^2 - (M_B - M_C)^2]}/2M_A$, and M_A, M_B, and M_C are the masses of the meson A, B, and C, respectively.

In order to determine the phase space and final state momenta, the masses of the initial state mesons involved in this work are taken to be the average values of Table I, and the masses of the final state mesons, except for the theoretical candidates of the final state mesons such as $D(2^1S_0)$, $D(2^3S_1)$, $D(1^3D_1)$, $D(1^3D_3)$, $D(1D)$, and $D'(1D)$, are taken from the PDG[4]. These theoretical candidates masses are: $M_{D(2^1S_0)} = (M_{D(2550)} + M_{D_J(2580)})/2$, $M_{D(2^3S_1)} = (M_{D^*(2600)} + M_{D_J^*(2650)})/2$, $M_{D(1^3D_1)} \simeq M_{D(1^3D_3)} = (M_{D^*(2760)} + M_{D_J^*(2760)})/2$, $M_{D_2(1D)} \simeq M_{D_2'(1D)} = (M_{D_J(2740)} + M_{D(2750)})/2$. The mixing angles θ_{nL} are taken from Table II, and the mixing angle of $D_{s1}(2460)$-$D_{s1}(2536)$ is solved to be $-37.5°$. There is only one free parameter γ in our calculations. We set $\gamma = 8.9$ by fitting to the following 34 two-body decay modes with specific branching ratios[4]: (1) $a_2(1320) \to \eta\pi$, (2) $a_2(1320) \to K\bar{K}$, (3) $f_2(1270) \to \pi\pi$, (4) $f_2(1270) \to K\bar{K}$, (5) $f_2'(1525) \to K\bar{K}$, (6) $f_2'(1525) \to \eta\eta$, (7) $\pi_2(1670) \to f_2(1270)\pi$, (8) $\pi_2(1670) \to \rho\pi$, (9) $\pi_2(1670) \to KK^*(892) + c.c.$, (10) $\pi_2(1670) \to \omega\rho$, (11) $\rho_3(1690) \to \omega\pi$, (12) $\rho_3(1690) \to \pi\pi$, (13) $\rho_3(1690) \to K\bar{K}$, (14) $f_4(2050) \to \pi\pi$, (15) $K^*(1410) \to K\pi$, (16) $K_0^*(1430) \to K\pi$, (17) $K_2^*(1430) \to K\pi$, (18) $K_2^*(1430) \to K^*(892)\pi$, (19) $K_2^*(1430) \to K\rho$, (20) $K_2^*(1430) \to K\omega$, (21) $K^*(1680) \to K\pi$, (22) $K^*(1680) \to K\rho$, (23) $K^*(1680) \to K^*(892)\pi$, (24) $K_3^*(1780) \to K\rho$, (25) $K_3^*(1780) \to K^*(892)\pi$, (26) $K_3^*(1780) \to K\pi$, (27) $K_3^*(1780) \to K\eta$, (28) $K_4^*(2045) \to K\pi$, (29) $K_4^*(2045) \to \phi K^*(892)$, (30) $D^*(2010)^+ \to D^0\pi^+$, (31) $D^*(2010)^+ \to D^+\pi^0$, (32) $\psi(3770) \to D\bar{D}$, (33) $\Upsilon(4S) \to$

TABLE IV: Decay widths of the $D(2550)/D_J(2580)$ as the $D(2^1S_0)$ in MeV.

$D^{*+}\pi^-$	85.20
$D^{*0}\pi^0$	43.22
$D_0^*(2400)^0\pi^0$	0.05
$D_0^*(2400)^+\pi^-$	0.09
$D^*\eta$	0.12
Total width	128.69
Experiment	$153.8 \pm 10.7 \pm 23.9$

B^+B^-, and (34) $\Upsilon(4S) \to B^0\bar{B}^0$. Here γ denotes the light nonstrange quark pair $u\bar{u}$ or $d\bar{d}$ creation strength and the strange quark pair $s\bar{s}$ creation strength $\gamma_{s\bar{s}}$ can be related by $\gamma_{s\bar{s}} = \gamma\frac{m_u}{m_s}$[33], where m_u and m_s are respectively the u-quark and s-quark masses employed in the GI quark model. Our value of γ is higher than that used by other groups such as[15, 30] by a factor of $\sqrt{96\pi}$ due to different field conventions, constant factor in the transition operator T, etc.

B. $D(2550)/D_J(2580)$

The decay widths of the $D(2550)/D_J(2580)$ as the $D(2^1S_0)$ compared with the experiment data are shown in Table IV. Under the $D(2^1S_0)$ assignment, the $D(2550)/D_J(2580)$ is predicted to have a total width of 128 MeV, which is in good agreement with $153.8 \pm 10.7 \pm 23.9$ MeV, the average value of the LHCb and BaBar measurements. The dominant decay channel of the $D(2^1S_0)$ is expected to be the $D^{*+}\pi^-$, which naturally explains that the $D(2550)$ and $D_J(2580)$ were observed in the $D^{*+}\pi^-$ channel. Therefore, both the masses and decays support that the $D(2550)/D_J(2580)$ is in fact the resonance $D(2^1S_0)$.

C. $D^*(2600)/D_J^*(2650)$

In Table V, we list the decay widths of the $D^*(2600)/D_J^*(2650)$ as the $D(2^3S_1)$ state. The predicted total width of the $D(2^3S_1)$ is 122 MeV, in good agreement with the average value of the LHCb and BaBar widths, $116.6 \pm 9.1 \pm 11.3$ MeV. The predicted branching ratio

$$\frac{\Gamma(D^*(2600) \to D^+\pi^-)}{\Gamma(D^*(2600) \to D^{*+}\pi^-)} = 0.43 \tag{10}$$

TABLE V: Decay widths of the $D^*(2600)/D_J^*(2650)$ as the $D(2^3S_1)$ in MeV.

$D^0\pi^0$	10.82
$D^+\pi^-$	21.66
D_sK	3.30
$D\eta$	4.73
$D^{*0}\pi^0$	25.20
$D^{*+}\pi^-$	49.82
$D^*\eta$	3.71
D_s^*K	0.55
$D_2^*(2460)^0\pi^0$	4.8×10^{-3}
$D_2^*(2460)^+\pi^-$	5.6×10^{-3}
$D_1(2430)^0\pi^0$	0.59
$D_1(2430)^+\pi^-$	1.16
$D_1(2420)^0\pi^0$	0.27
$D_1(2420)^+\pi^-$	0.50
Total width	122.30
Experiment	$116.6 \pm 9.1 \pm 11.3$

is consistent with the BaBar result of $0.32 \pm 0.02 \pm 0.09$[2]. Also, the expected dominant decay modes of the $D(2^3S_1)$ are $D^*\pi$ and $D\pi$, which is consistent with the observation. So, the masses and decays support that the $D^*(2600)/D_J^*(2650)$ is the state $D(2^3S_1)$.

D. $D_J(2740)/D(2750)$

The decay widths of the $D_J(2740)/D(2750)$ as the $D_2(1D)$ and $D_2'(1D)$ are listed in Table VI. The total width for the $D_2(1D)$ with a mass around 2750 MeV is expected to be about 280 MeV, much larger than the LHCb and BaBar results, which excludes the assignment of the $D_J(2740)/D(2750)$ as the $D_2(1D)$ state. With the $D_2'(1D)$ assignment to the $D_J(2740)/D(2750)$, its total width is predicted to be 109 MeV, which is reasonably close to the LHCb and BaBar experimental average of $72.1 \pm 7.4 \pm 13.7$ MeV, and consistent with the LHCb width of $73.2 \pm 13.4 \pm 25.0$ MeV[1]. In other approaches such as the chiral quark model[6, 7] and the heavy quark effective theory[18], it is also found that under the $D_2'(1D)$ assignment, the $D_J(2740)/D(2750)$ width can be reasonably accounted for.

It is noted that the mass prediction of the GI quark model for the $D_2'(1D)$ differs by around 100 MeV from the observed mass of the $D_J(2740)/D(2750)$. This discrepancy between the GI quark model and the experiment maybe result from that the coupled channel effects (also

called hadron loop effects) were neglected in the GI quark model. The coupled channel effects can give rise to mass shifts to the bare hadron states. The mass shifts induced by the coupled channel effects can present a better description of the D, D_s, charmonium, and bottomonium states[17, 34]. Other approaches such as the nonrelativistic quark model[12], the relativistic quark model[23], and the Blankenbecler-Sugar equation[35] consistently predict that the $D_2'(1D)$ mass is very close to the $D_J(2740)/D(2750)$ mass, which make the $D_2'(1D)$ assignment to the $D_J(2740)/D(2750)$ possible based on its mass.

Therefore, identification of the $D_J(2740)/D(2750)$ as the $D_2'(1D)$ state seems favored by the available experimental data. The conclusion that the $D_J(2740)/D(2750)$ can be explained as the $D_2'(1D)$ has been suggested by Refs.[6–10, 12, 14, 18].

In the heavy quark effective theory, the $D_2(1D)$ and $D_2'(1D)$ can be grouped into the $(1^-, 2^-)_{j=\frac{3}{2}}$ and $(2^-, 3^-)_{j=\frac{5}{2}}$ doublets, where j is the total angular momentum of the light quark. In the heavy quark limit, there are two mixing angle[36]: one is -50.8° for which the $D_2'(1D)$ belongs to the $j=\frac{5}{2}$ states, and the other is 39.2° for which the $D_2(1D)$ belongs to the $j=\frac{3}{2}$ states. Among these two 2^- charmed mesons, the decay width is expected to be broader for $j=\frac{3}{2}$ than for $j=\frac{5}{2}$.

The total widths of the $D_J(2740)/D(2750)$ as the $D_2(1D)$ and $D_2'(1D)$ dependence on the mixing angle θ_{1D} are also depicted in Fig. 2. It is clear that for the θ_{1D} lying around $(-20^\circ \sim -80^\circ)$, the $D_2(1D)$ is much broader than the $D_2'(1D)$. Our predicted $\theta_{1D} = -38.2^\circ$ is close to -50.8° while far from 39.2°, so, with the $D_2'(1D)$ assignment, $D_J(2740)/D(2750)$ corresponds to the 2^- charmed meson belonging to the $(2^-, 3^-)_{j=\frac{5}{2}}$ doublet.

The dominant decay channels of the $D_2'(1D)$ are expected to be $D^*\pi$, $D\rho$, and $D\omega$, while the dominant decay channels of the $D_2(1D)$ are $D^*\pi$, $D^*\eta$, $D_2^*\pi$. The $D_2^*\pi$ channel is the most dominant decay mode of the $D_2(1D)$, and therefore is the ideal decay channel to further experimental search for the partner of the $D_J(2740)/D(2750)$.

E. $D^*(2760)/D_J^*(2760)$

The decay widths of the $D^*(2760)/D_J^*(2760)$ as the $D(1^3D_1)$ and $D(1^3D_3)$ are listed in Table VII. Our results show the possibility of the $D^*(2760)/D_J^*(2760)$ being the $D(1^3D_1)$ can be excluded because the theoretical total width is 366 MeV, much larger than the LHCb and BaBar results. With the $D(1^3D_3)$ assignment, the $D^*(2760)/D_J^*(2760)$ is expected to have a

TABLE VI: Decay widths of the $D_J(2740)/D(2750)$ as the $D_2(1D)$ and $D_2'(1D)$ in MeV.

Channel	$D_2(1D)$	$D_2'(1D)$
$D^{*0}\pi^0$	38.21	7.00
$D^{*+}\pi^-$	75.98	13.50
$D^*\eta$	13.34	0.93
D_s^*K	6.40	0.35
$D_2^*(2460)^0\pi^0$	48.57	2.36
$D_2^*(2460)^+\pi^-$	96.17	4.66
$D_1(2430)^0\pi^0$	0.03	0.02
$D_1(2430)^+\pi^-$	0.05	0.04
$D_1(2420)^0\pi^0$	0.10	0.31
$D_1(2420)^+\pi^-$	0.19	0.57
$D^0\rho^0$	0.23	20.78
$D^+\rho^-$	0.39	39.39
$D\omega$	0.18	19.34
$D_0^*(2400)^0\pi^0$	0.02	0.11
$D_0^*(2400)^+\pi^-$	0.02	0.07
Total width	279.90	109.43
Experiment	$72.1 \pm 7.4 \pm 13.7$	

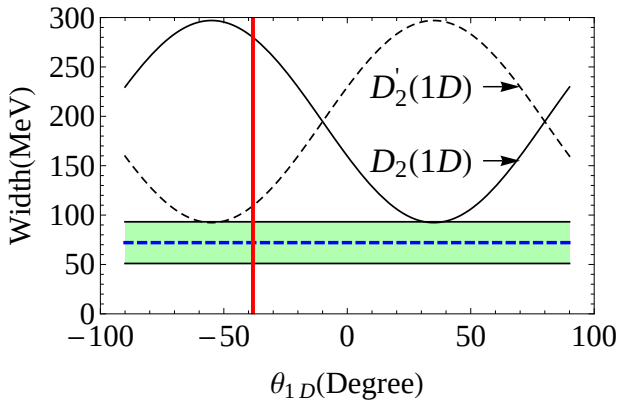

FIG. 2: Total decay width of $D_J(2740)/D(2750)$ as the $D_2(1D)$ and $D_2'(1D)$ versus the mixing angle. The blue dashed line with a green band denotes the LHCb and BaBar experimental average. The vertical red solid line corresponds to the mixing angle $\theta_{1D} = -38.2^\circ$ obtained in Sec. II.

width of about 28 MeV, which is somewhat lower than the average value of the LHCb and BaBar results but roughly consistent with the LHCb width of $74.4 \pm 3.4 \pm 37.0$ MeV[1]. The discrepancy between the predicted width of the $^3P_0$ model for the $D(1^3D_3)$ and the average width of the $D^*(2760)$ and $D_J^*(2760)$ could arise from the inherent uncertainty of the $^3P_0$ model itself. As pointed out by Ref.[29], the $^3P_0$ model is a coarse model of the complicated strong decay theory and the best it can hope for is to predict a decay width to within a factor of 2.

Apart from the $^3P_0$ model, other approaches such as the chiral quark model[6, 7] and the heavy quark effective theory[18] have been used to discuss the possibility of the $D^*(2760)/D_J^*(2760)$ being the $D(1^3D_3)$. In Refs.[6, 7], the $D^*(2760)/D_J^*(2760)$ as the $D(1^3D_3)$ is expected to have a width of about 68 MeV, consistent with the experiment. In Ref.[18], the $D^*(2760)/D_J^*(2760)$ as the $D(1^3D_3)$ is expected to have a width of about 40 MeV, very close to the lower limit of 67.6±3.1±18.6 MeV, the average value of the LHCb and BaBar results. So, the measured widths in fact strongly prefer the $D(1^3D_3)$ over the $D(1^3D_1)$ assignment to the $D^*(2760)/D_J^*(2760)$.

Similar to the case of the $D_J(2740)/D(2750)$, the observed $D^*(2760)/D_J^*(2760)$ mass is about 70 MeV lower than the GI quark model mass prediction for the $D(1^3D_3)$. As mentioned in subsection D, the coupled channel effects being neglected in the GI quark model maybe cause the discrepancy between the experiment and the GI quark model. Other model calculations such as nonrelativistic quark model[12], coupled channel effects[17], the relativistic quark model[23], and Regge phenomenology[37] show that the $D(1^3D_3)$ mass is close to the $D^*(2760)/D_J^*(2760)$ mass, which makes the $D(1^3D_3)$ assignment to the $D^*(2760)/D_J^*(2760)$ plausible based on its mass.

With the assignment of the $D(2750)$ as the $D_2'(1D)$, the predicted width ratio is

$$\frac{\Gamma(D^*(2760)\to D^+\pi^-)}{\Gamma(D(2750)\to D^{*+}\pi^-)}=\begin{cases}0.68, D^*(2760)=D(1^3D_3)\\ 4.09, D^*(2760)=D(1^3D_1)\end{cases}. \tag{11}$$

Comparison of the theoretical ratio and the corresponding BaBar experimental ratio of $0.42\pm0.05\pm0.11$[2] also strongly prefers the $D(1^3D_3)$ over the $D(1^3D_1)$ assignment to the $D^*(2760)$. The suggestion that the $D^*(2760)/D_J^*(2760)$ can be identified as the $D(1^3D_3)$ has been proposed in Refs.[6–12, 14, 18] based on its mass and width.

The decay behavior of the $D(1^3D_1)$ is remarkably different from those of the $D(1^3D_3)$. The main decay modes of the $D(1^3D_1)$ are expected to be $D\pi$, $D^*\pi$, $D_1(2420)\pi$, $D_1(2430)\pi$, $D\rho$, $D\eta$, D_sK, and $D\omega$, while the $D(1^3D_3)$ is expected to mainly decay to $D\pi$ and $D^*\pi$, consistent with the observation of the $D_J^*(2760)$ in both the $D\pi$ and $D^*\pi$ channels. Further experimental analysis of the $D_1(2420)\pi$, $D_1(2430)\pi$, $D\rho$, $D\eta$, D_sK, and $D\omega$ systems would be helpful to search for the candidate for the $D(1^3D_1)$.

TABLE VII: Decay widths of the $D^*(2760)/D_J^*(2760)$ as the $D(1^3D_1)$ and $D(1^3D_3)$ in MeV.

Channel	$D(1^3D_1)$	$D(1^3D_3)$
$D^0\pi^0$	27.61	4.77
$D^+\pi^-$	55.24	9.29
D_sK	9.47	0.22
$D\eta$	13.69	0.77
$D^{*0}\pi^0$	13.56	3.81
$D^{*+}\pi^-$	26.98	7.28
$D^*\eta$	4.95	0.26
D_s^*K	2.54	0.04
$D_2^*(2460)^0\pi^0$	0.23	0.22
$D_2^*(2460)^+\pi^-$	0.43	0.40
$D_1(2430)^0\pi^0$	13.76	0.13
$D_1(2430)^+\pi^-$	27.54	0.24
$D_1(2420)^0\pi^0$	46.92	0.01
$D_1(2420)^+\pi^-$	93.43	0.02
$D^0\rho^0$	7.71	0.24
$D^+\rho^-$	14.75	0.42
$D\omega$	7.28	0.20
$D(2^1S_0)^0\pi^0$	0.17	2.1×10^{-4}
$D(2^1S_0)^+\pi^-$	0.31	3.5×10^{-4}
Total width	366.58	28.32
Experiment	$67.6\pm3.1\pm18.6$	

F. $D_J(3000)$

The decay widths of the $D_J(3000)$ as the $D(3^1S_0)$, $D_1(2P)$, $D_1(2P)$, $D_3(1F)$, and $D_3'(1F)$ are listed in Table VIII. It is clear that the most favorable assignment of the $D_J(3000)$ is the $D(3^1S_0)$, since the predicted $D(3^1S_0)$ total width of 180 MeV agrees quite well with the experimental data of 188.1 ± 44.8 MeV while the total widths for other assignments are far from the measurement. The main decay modes of the $D(3^1S_0)$ are expected to be the $D_2^*\pi$, $D^*\pi$, $D^*\rho$, $D^*\omega$, and $D(2^3S_1)\pi$.

Our most favorable assignment of the $D_J(3000)$ is the $D(3^1S_0)$, which is inconsistent with the $D_1(2P)$ assignment proposed by Refs.[13, 14] and the $D_3'(1F)$ assignment proposed by Ref.[14]. The partial widths of the $D(2^3S_1)\pi$, $D(1^3D_1)\pi$, $D(1^3D_3)\pi$, $D_2(1D)\pi$, and $D_2'(1D)\pi$ are considered in our calculations but neglected in Refs.[13, 14]. Our results show that the total contributions of these channels are large for the $D(3^1S_0)$, $D_1(2P)$, $D_1'(2P)$, and $D_3(1F)$ but tiny for the $D_3'(1F)$. Without doubt, further experimental studies of the $D_J(3000)$ on the

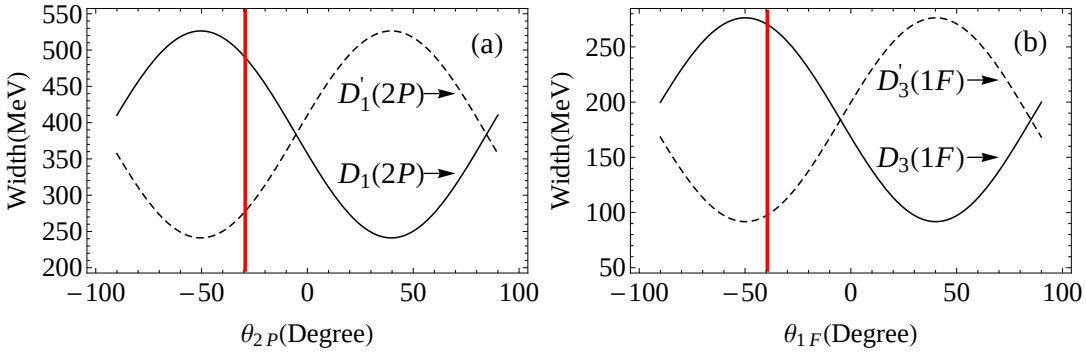

FIG. 3: Total widths of the $D_1(2P)$, $D_1'(2P)$, $D_3(1F)$, and $D_3'(1F)$ versus the mixing angle. The vertical red solid line corresponds to the mixing angle obtained in Sec. II: $\theta_{2P} = -29.4°$ and $\theta_{1F} = -39.5°$.

$D_1(2420)\pi$, $D_1(2430)\pi$, $D_2(1D)\pi$, and $D_2'(1D)\pi$ channels will be useful to check our present assignment because these decay modes are forbidden for the $D(3^1S_0)$ while allowable for the $D_1(2P)$, $D_1'(2P)$, $D_3(1F)$, and $D_3'(1F)$.

The total widths of the $D_1(2P)$, $D_1'(2P)$, $D_3(1F)$, and $D_3'(1F)$ dependence on the mixing angles are depicted in Fig. 3, which will be helpful to determine the mixing angles θ_{2P} and θ_{1F} based on the measured widths.

G. $D_J^*(3000)$

The decay widths of the $D_J^*(3000)$ as the $D(3^3S_1)$, $D(2^3P_0)$, $D(2^3P_2)$, $D(1^3F_2)$, and $D(1^3F_4)$ are listed in Table IX. The predicted total widths indicate that the assignments of the $D_J^*(3000)$ as the $D(2^3P_0)$, $D(2^3P_2)$, and $D(1^3F_2)$ can be ruled out because the corresponding widths are much larger than the LHCb measurement of 110.5 ± 11.5 MeV[1]. Among the remaining two possible assignments of the $D_J^*(3000)$, the measured width prefers the $D(1^3F_4)$ over the $D(3^3S_1)$, since the $D(3^3S_1)$ width is 157 MeV, somewhat larger than the experimental data, while the $D(1^3F_4)$ width is 103 MeV, in good agreement with the experimental data. The main decay modes of the $D(1^3F_4)$ are predicted to include the $D\pi$, $D^*\pi$, $D^*\rho$, $D^*\omega$.

Our most favorable assignment of the $D_J^*(3000)$ is the $D(1^3F_4)$. Ref.[13] suggests that the $D_J^*(3000)$ can be explained as the $D(2^3P_0)$ and Ref.[14] assigns the $D_J^*(3000)$ as the $D(1^3F_2)$ or $D(1^3F_4)$. Obviously, the theoretical interpretations on the $D_J^*(3000)$ are not completely consistent with each other. The partial widths of the $D(2^1S_0)\pi$, $D(2^3S_1)\pi$, $D(1^3D_1)\pi$, $D(1^3D_1)\pi$, $D_2(1D)\pi$, and $D_2'(1D)\pi$ are considered in our present calculations while neglected

in Refs.[13, 14]. Our results indicate that total contributions of these channels are large for the $D(3^1S_0)$, $D(2^3P_0)$, $D(2^3P_2)$, and $D(1^3F_2)$ while tiny for the $D(1^3F_4)$. Further experimental information of the $D_J^*(3000)$ in these channels will be helpful to test our present assignment.

IV. SUMMARY

In order to understand the possible quark-model assignments of the BaBar and LHCb charmed states, we apply the GI quark model to calculate the $1S$, $2S$, $3S$, $1P$, $2P$, $3P$, $1D$, $2D$, $3D$, $1F$, $2F$, $3F$, $1G$, and $2G$-wave charmed meson spectroscopy. Our mass predictions, together with the expectations of some other relativistic quark models, present the mass ranges of the D mesons. From these predicted mass ranges and the parity information, we tentatively give the possible quark-model assignments for the BaBar and LHCb charmed states.

To clarify these possible assignments, we then evaluate the strong decay behaviors of these charmed states in the framework of the $^3P_0$ model, where the GI quark model wave functions are employed. In our calculations, the only one free parameter γ, the quark pair creation strength, is obtained by fitting to 34 decay modes with specific branching ratios.

We calculate the two-body strong decay properties of the $2S$, $3S$, $2P$, $1D$, and $1F$-wave charmed mesons. Comparison of the strong decay predictions and the measured decay properties, we find that the observed decay properties of these charmed states can be reasonably explained. Therefore, we tend to conclude that the $D(2550)/D_J(2580)$, $D^*(2600)/D_J^*(2650)$, $D_J(2740)/D(2750)$, $D^*(2760)/D_J^*(2760)$, $D_J(3000)$, and $D_J^*(3000)$ can be identified as the $D(2^1S_0)$, $D(2^3S_1)$, $D_2'(1D)$, $D(1^3D_3)$, $D(3^1S_0)$, and $D(1^3F_4)$, respectively. Further experimental information on the spin-parity and branching ratios of these charmed states will provide a useful consistency check for our present assignments.

Our predictions on the masses and strong decays for the $D(3^3S_1)$, $D_2(1D)$, $D(1^3D_1)$, $D(2^3P_0)$, $D(2^3P_2)$, $D_1(2P)$, $D_1'(2P)$, $D(1^3F_2)$, $D_3(1F)$, and $D_3'(1F)$ will be useful to search for the corresponding charmed mesons experimentally.

ACKNOWLEDGEMENTS

This work is partly supported by the National Natural Science Foundation of China under

Grant No. 11105126.

---

[1] R. Aaij *et al.* (LHCb Collaboration), JHEP **1309**, 145 (2013).

[2] P. del Amo Sanchez *et al.* (BaBar Collaboration), Phys. Rev. D **82**, 111101 (2010).

[3] S. Godfrey and J. Napolitano, Rev. Mod. Phys. **71**, 1411 (1999).

[4] J. Beringer *et al.* (Particle Data Group), Phys. Rev. D **86**, 010001 (2012).

[5] X. H. Zhong and Qiang Zhao, Phys. Rev. D **78**, 014029 (2008);

[6] X. -H. Zhong, Phys. Rev. D **82**, 114014 (2010).

[7] L. Y. Xiao and X. H. Zhong, arXiv:1407:7408

[8] Z. -G. Wang, Phys. Rev. D **83**, 014009 (2011).

[9] P. Colangelo, F. De Fazio, F. Giannuzzi, and S. Nicotri, Phys. Rev. D **86** 054024 (2012).

[10] Z. -G. Wang, Phys. Rev. D **88**, 114003 (2013).

[11] Z. -F. Sun, J. -S. Yu, X. Liu and T. Matsuki, Phys. Rev. D **82**, 111501 (2010).

[12] D. -M. Li, P. -F. Ji and B. Ma, Eur. Phys. J. C **71**, 1582 (2011).

[13] Y. Sun, X. Liu and T. Matsuki, Phys. Rev. D **88**, 094020 (2013).

[14] G. Yu, Z. -G. Wang and Z. Li, arXiv:1402.5955 [hep-ph].

[15] F. E. Close and E. S. Swanson, Phys. Rev. D **72**, 094004 (2005).

[16] J. Segovia, D. R. Entem and F. Fernandez, Phys. Lett. B **715**, 322 (2012).

[17] Z. Y. Zhou, Z. G. Xiao, Phys. Rev. D **84**, 034023 (2011).

[18] B. Chen, L. Yuan, and A. Zhang, Phys. Rev. D **83**, 114025 (2011).

[19] Z. H. Wang, G. L. Wang, J. M. Zhang, and T. H. Wang, J. Phys. G **39**, 085006 (2012).

[20] S. Godfrey and N. Isgur, Phys. Rev. D **32**, 189 (1985).

[21] S. Godfrey and R. Kokoski, Phys. Rev. D **43**, 1679 (1991).

[22] E. Hiyama, Y. Kino and M. Kamimura, Prog. Part. Nucl. Phys. **51**, 223 (2003).

[23] J. Zeng, J. W. Van Orden, and W. Roberts, Phys. Rev. D **52**, 5229 (1995).

[24] M. Di Pierro and E. Eichten, Phys. Rev. D **64**, 114004 (2001).

[25] D. Ebert, R. N. Faustov, and V. O. Galkin, Eur. Phys. J. C **66**, 197 (2010).

[26] L. Micu, Nucl. Phys. B **10**, 521, (1969).

[27] A. Yaounc, L. Oliver, O. Pene, and J-C. Raynal, *Hardon Transitons in the quark model* (Gordon and Breach, New York, 1988).

[28] W. Roberts and B. Silverstr-Brac, Few-Body Syst. **11**, 171 (1992).

[29] H. G. Blundell, Ph. D. thesis, Carleton Universtiy, 1996, arXiv: hep-ph/9608473.

[30] E. S. Ackleh, T. Barnes, and E. S. Swanson, Phys. Rev. D **54**, 6811 (1996); T. Barnes, F. E. Close, P. R. Page, and E. S. Swanson, Phys. Rev. D **55**, 4157 (1997), T. Barnes, N. Black, and P. R. Page, Phys. Rev. D **68**, 054014 (2003).

[31] D. M. Li and B. Ma, Phys. Rev. D **77**, 074004 (2008); D. M. Li and B. Ma, Phys. Rev. D **77**, 094021 (2008); D. M. Li and E. Wang, Eur. Phys. J. C **63**, 297 (2009).

[32] C. Hayne and N. Isgur, Phys. Rev. D **25**, 1944 (1982).

[33] A. Le Yaouanc, L. Oliver, O. Pene, and J. C. Raynal, Phys. Lett. B **72**, 57 (1977).

[34] K. Heikkila, N. A. Tornqvist, and S. Ono, Phys. Rev. D **29**, 110 (1984); E. van Beveren and G. Rupp, Phys. Rev. Lett. **91**, 012003 (2003);
Y. A. Simonov and J. A. Tjon, Phys. Rev. D **70**, 114013 (2004);
D. S. Hwang and D. W. Kim, Phys. Lett. B **601**, 137 (2004);
D. Becirevic, S. Fajfer, and S. Prelovsek, Phys. Lett. B **599**, 55 (2004); E. S. Swanson, Phys. Rep. **429**, 243 (2006);
M. R. Pennington and D. J. Wilson, Phys. Rev. D **76**, 077502 (2007);
T. Barnes and E. S. Swanson, Phys. Rev. C **77**, 055206 (2008);
F. K. Guo, S. Krewald, and U. G. Meissner, Phys. Lett. B **665**, 157 (2008);
J. F. Liu and G. J. Ding, Eur. Phys. J. C **72**, 1981 (2012).

[35] T. A. Lahde, C. J. Nyfalt, and D. O. Riska, Nucl. Phys. A **674**, 141 (2000).

[36] R. N. Cahn and J. D. Jackson, Phys. Rev. D **68**, 037502 (2003); T. Matsuki, T. Morii, and K. Seo, Prog. Theor. Phys. **124**, 285 (2010).

[37] D. M. Li, B. Ma, and Y. H. Liu, Eur. Phys. J. C **51**, 359 (2007).

TABLE VIII: Decay widths of $D_J(3000)$ with several possible assignments in MeV. A dash indicates that a decay mode is forbidden.

	$D(3^1S_0)$	$D_1(2P)$	$D_1'(2P)$	$D_3(1F)$	$D_3'(1F)$
$D^0\rho^0$	0.13	26.99	1.16	1.38	13.40
$D^+\rho^-$	0.36	53.14	1.98	2.60	26.34
$D\omega$	0.20	26.55	0.95	1.28	13.15
$D_0^*(2400)^0\pi^0$	1.67	1.93	0.94	0.12	0.29
$D_0^*(2400)^+\pi^-$	4.91	4.06	1.98	0.13	0.29
$D_0^*(2400)\eta$	3.56	0.84	0.40	3.5×10^{-3}	6.4×10^{-3}
$D_2^*(2460)^0\pi^0$	13.77	40.40	6.98	33.26	1.04
$D_2^*(2460)^+\pi^-$	27.07	80.53	13.70	66.04	2.07
$D^{*0}\pi^0$	8.72	18.79	15.64	16.18	4.76
$D^{*+}\pi^-$	16.67	36.92	31.25	32.18	9.20
$D^*\eta$	0.55	4.39	6.88	6.59	0.83
$D^*\eta'$	0.07	3.80	0.95	2.0×10^{-3}	5.4×10^{-5}
$D^{*0}\rho^0$	15.53	29.47	32.84	5.87	5.46
$D^{*+}\rho^-$	32.13	57.33	62.68	11.07	10.30
$D^*\omega$	16.18	28.70	31.31	5.53	5.14
D_s^*K	5.7×10^{-3}	0.95	4.14	2.88	0.20
D_sK^*	1.41	1.48	10.41	3.4×10^{-3}	0.48
$D_{s0}^*(2317)K$	4.09	1.19	0.74	6.7×10^{-3}	0.02
$D_1(2430)^0\pi^0$	–	0.11	0.15	0.02	4.6×10^{-3}
$D_1(2430)^+\pi^-$	–	0.21	0.29	0.04	9.1×10^{-3}
$D_1(2420)^0\pi^0$	–	2.77	11.32	0.29	0.79
$D_1(2420)^+\pi^-$	–	5.53	22.62	0.56	1.52
$D_1(2420)\eta$	–	7.2×10^{-3}	0.03	4.0×10^{-8}	9.9×10^{-8}
$D_{s1}(2460)K$	–	2.1×10^{-4}	0.01	1.3×10^{-8}	2.7×10^{-6}
$D(2^3S_1)^0\pi^0$	11.03	20.90	5.93	0.56	0.02
$D(2^3S_1)^+\pi^-$	21.86	42.04	11.84	1.10	0.04
$D(1^3D_1)^0\pi^0$	0.16	0.02	0.02	6.7×10^{-5}	1.2×10^{-5}
$D(1^3D_1)^0\pi^-$	0.29	0.32	0.04	1.2×10^{-4}	2.3×10^{-5}
$D(1^3D_3)^0\pi^0$	8.1×10^{-2}	0.23	0.01	27.77	0.77
$D(1^3D_3)^+\pi^-$	0.01	0.41	0.02	54.80	1.53
$D_2(1D)^0\pi^0$	–	4.9×10^{-3}	0.01	3.9×10^{-3}	2.1×10^{-3}
$D_2(1D)^+\pi^-$	–	9.1×10^{-3}	0.02	7.1×10^{-3}	3.9×10^{-3}
$D_2'(1D)^0\pi^0$	–	0.03	0.14	0.01	0.03
$D_2'(1D)^+\pi^-$	–	0.06	0.25	0.02	0.05
Total width	180.39	489.85	277.62	270.33	97.75
Experiment			188.1 ± 44.8		

TABLE IX: Decay widths of the $D_J^*(3000)$ with several possible assignments in MeV. A dash indicates that a decay mode is forbidden.

	$D(3^3S_1)$	$D(2^3P_0)$	$D(2^3P_2)$	$D(1^3F_2)$	$D(1^3F_4)$
$D^0\pi^0$	4.72	27.98	0.62	9.52	3.37
$D^+\pi^-$	9.29	55.48	1.30	19.03	6.59
$D\eta$	1.39	9.75	0.93	4.72	0.83
$D^0\rho^0$	0.17	–	12.79	5.94	1.25
$D^+\rho^-$	0.25	–	25.40	11.71	2.40
$D\omega$	0.12	–	12.72	5.85	1.19
$D\eta'$	6.4×10^{-3}	0.18	0.84	1.53	0.03
$D_2^*(2460)^0\pi^0$	6.87	–	6.23	4.40	0.86
$D_2^*(2460)^+\pi^-$	13.60	–	12.36	8.73	1.66
$D^{*0}\pi^0$	6.59	–	3.91	7.02	3.21
$D^{*+}\pi^-$	12.76	–	7.98	13.99	6.20
$D^*\eta$	0.85	–	2.97	3.02	0.57
$D^*\eta'$	0.37	–	0.13	0.06	1.2×10^{-4}
$D^{*0}\rho^0$	8.93	73.53	19.78	3.99	18.85
$D^{*+}\rho^-$	19.19	141.85	38.52	7.53	36.15
$D^*\omega$	9.68	70.98	19.29	3.76	18.09
$D_1(2430)^0\pi^0$	1.62	19.46	4.91	8.11	0.63
$D_1(2430)^+\pi^-$	3.25	39.01	9.81	16.23	1.25
$D_1(2430)\eta$	1.79	2.01	0.43	0.53	4.8×10^{-4}
$D_1(2420)^0\pi^0$	4.32	39.21	3.25	26.52	0.04
$D_1(2420)^+\pi^-$	8.58	78.38	6.33	52.82	0.08
$D_1(2420)\eta$	0.62	3.86	0.03	2.15	1.5×10^{-6}
D_sK	0.48	2.52	1.09	2.61	0.21
D_s^*K	0.08	–	2.22	1.41	0.12
D_sK^*	0.74	–	1.21	0.35	6.2×10^{-3}
$D_s^*K^*$	0.09	3.78	6.68	7.6×10^{-5}	4.7×10^{-4}
$D_{s1}(2460)K$	2.65	1.77	0.83	0.26	1.6×10^{-3}
$D(2^1S_0)^0\pi^0$	4.44	21.57	2.78	1.23	0.03
$D(2^1S_0)^+\pi^-$	8.90	43.56	5.49	2.43	0.07
$D(2^3S_1)^0\pi^0$	8.02	–	1.93	0.32	0.01
$D(2^3S_1)^+\pi^-$	15.98	–	3.80	0.62	0.02
$D(1^3D_1)^0\pi^0$	0.07	–	6.0×10^{-4}	1.9×10^{-3}	1.7×10^{-6}
$D(1^3D_1)^0\pi^-$	0.12	–	1.1×10^{-3}	3.5×10^{-3}	3.1×10^{-6}
$D(1^3D_3)^0\pi^0$	0.02	–	0.15	0.05	0.05
$D(1^3D_3)^+\pi^-$	0.04	–	0.27	0.09	0.10
$D_2(1D)^0\pi^0$	0.32	0.02	0.51	1.59	5.6×10^{-5}
$D_2(1D)^+\pi^-$	0.61	0.03	1.00	3.17	1.2×10^{-4}
$D_2'(1D)^0\pi^0$	0.06	1.49	0.09	37.24	5.9×10^{-3}
$D_2'(1D)^+\pi^-$	0.11	2.82	0.17	74.35	0.01
Total width	157.69	639.26	218.76	342.87	103.90
Experiment			110.5 ± 11.5		